

The Mean Meridional Circulation of the Atmosphere Using the Mass above Isentropes as the Vertical Coordinate

GANG CHEN

Department of Earth and Atmospheric Sciences, Cornell University, Ithaca, New York

(Manuscript received 29 August 2012, in final form 18 December 2012)

ABSTRACT

The mean meridional circulation of the atmosphere is presented using the mass (more specifically, the pressure corresponding to the mass) above the isentrope of interest as the vertical coordinate. In this vertical coordinate, the mass-weighted mean circulation is exactly balanced by entropy sources and sinks with no eddy flux contribution as in the isentropic coordinate, and the coordinate can be readily generalized to the mass above moist isentropes or other quasi-conservative tracers by construction. The corresponding Eliassen–Palm (EP) flux divergence for the zonal-mean angular momentum is formulated in a hybrid isobaric–isentropic form, extending the conventional transformed Eulerian-mean (TEM) formulation to finite-amplitude non-geostrophic eddies on the sphere. In the small-amplitude limit, the hybrid isobaric–isentropic formulation reduces to the TEM formulation.

Applying to the NCEP–U.S. Department of Energy (DOE) Reanalysis 2, the new formulation resolves the deficiency of the conventional TEM formulation for the near-surface flow, where the isentropic surface intersects the ground, and the mean circulation agrees well with the TEM above the near-surface layer. In the small-amplitude limit, this improvement near the surface can be partially attributed to the isentropic static stability over the isobaric counterpart, as the mass density in the near-surface isentropic layers gradually approaches zero. Also, the mean mass streamfunction can be approximately obtained from the EP flux divergence except for the deep tropics or the near-surface flow, highlighting the dominant control of potential vorticity mixing for the subtropics-to-pole mean circulations. It is then expected to provide a valuable diagnostic framework not only for global circulation theory, but also for atmospheric transport in the troposphere.

1. Introduction

The global atmospheric circulation transports momentum, energy, moisture, and chemical constituents both horizontally and vertically, and consequently impacts both global and regional climate. The conventional Eulerian-mean circulation, averaged at constant pressure or height, displays a three-cell pattern in each hemisphere, with a tropical Hadley cell, a midlatitude Ferrel cell, and a polar cell (e.g., Peixoto and Oort 1992). By contrast, to the extent that an isentropic surface can be regarded as a material surface in the absence of diabatic heating or diffusion, the mean circulation averaged at constant potential temperature can approximate the Lagrangian motion of an air parcel. In the isentropic coordinates, the mean circulation exhibits one equator-to-pole cell, with

a poleward circulation in the upper troposphere and an equatorward return flow near the surface (e.g., Townsend and Johnson 1985; Tung 1986; Iwasaki 1989; Jukes et al. 1994; Held and Schneider 1999; Tanaka et al. 2004; Czaja and Marshall 2006; Pauluis et al. 2008, 2010). The upward branch of the isentropic circulation corresponds to diabatic heating in the tropics and the descending branch in the polar region is accompanied by radiative cooling.

The isentropic mean circulation is approximated in more familiar geometric coordinates by the transformed Eulerian-mean (TEM) residual circulation, resulting in an analogous single-cell circulation from equator to pole (e.g., Andrews and McIntyre 1976, 1978; Edmon et al. 1980; Tung 1986; Andrews et al. 1987; Iwasaki 1989; McIntosh and McDougall 1996; Jukes 2001; Plumb and Ferrari 2005; Pauluis et al. 2011). In the TEM formulation, the residual circulation is generally formulated as the Eulerian-mean circulation plus an eddy term that corresponds to a wave-driven Stokes drift in the small-amplitude limit. Held and Schneider (1999) showed that

Corresponding author address: Gang Chen, Bradfield Hall 1115, Dept. of Earth and Atmospheric Sciences, Cornell University, Ithaca, NY 14853.
E-mail: gc352@cornell.edu

owing to nearly neutral static stability in the boundary layer, the equatorward flow in the conventional TEM framework of Andrews and McIntyre (1976) does not close at the ground, implying a very thin near-surface layer. This contrasts with the isentropic circulation that an equatorward flow exists in a finite-depth isentropic layer where the layer intersects with the ground (Held and Schneider 1999). Several alternative approximations of isentropic circulation were proposed, such as considering the meridional temperature gradient rather than the static stability in the original TEM formulation (Held and Schneider 1999) or partitioning the eddy fluxes into adiabatic and diabatic components (Plumb and Ferrari 2005). More recently, Pauluis et al. (2011) generalize the TEM formulation to nonmonotonic vertical coordinates by assuming a Gaussian joint distribution for the meridional wind and the state variable of interest.

Another important aspect of the TEM circulation is the corresponding eddy forcing of angular momentum transport. Under the quasigeostrophic approximation, the eddy forcing of angular momentum can be expressed as the well-known Eliassen–Palm (EP) flux divergence (e.g., Andrews and McIntyre 1976; Edmon et al. 1980), corresponding to the nonacceleration theorem (e.g., Charney and Drazin 1961). This relationship can be generalized to finite-amplitude eddies in the isentropic coordinates on the sphere, treating the isentropic mean circulation as the analog for the TEM residual circulation (e.g., Andrews 1983; Tung 1986; Iwasaki 1989, 1998). Further, using a coordinate-independent formulation of Andrews and McIntyre (1978), Plumb and Ferrari (2005) generalized the TEM theory for non-quasigeostrophic eddies in geometric coordinates, and within this framework, Kuo et al. (2005) analyzed the potential vorticity (PV) homogenization in a cylinder flow.

In this paper, we present a new hybrid isobaric–isentropic diagnostic of the mean circulation and corresponding eddy forcing using the mass above the isentropes at each latitude and time as the vertical coordinate. Given the fact that the mass above the isentropic surface decreases monotonically with increasing potential temperature (i.e., positive static stability), we can define a new vertical coordinate corresponding to the mass above the isentrope of interest, termed as “equivalent pressure,” analogous to the familiar concept of equivalent latitude (Butchart and Remsberg 1986). This is essentially equivalent to changing the vertical coordinate of the isentropic formulation from potential temperature to the isentropic zonal-mean pressure in Iwasaki (1989) and Iwasaki (1998). However, our hybrid diagnostic framework is built on the pressure coordinates and can be readily generalized

from dry isentropes to other quasi-conservative quantities by construction. Further, the relationship between the TEM and isentropic circulation is clearer in our hybrid formulation, and the problem of conventional TEM streamfunction near the ground can be remedied, at least partially, by replacing the Eulerian static stability with isentropic static stability.

The paper is organized as follows. We first introduce the basic formulations of hybrid isobaric–isentropic diagnostics in section 2. The isentropic mass-weighted mean static stability and meridional wind are discussed in comparison with their isobaric counterparts in section 3. In section 4, the thermodynamic balance between the mean circulation and entropy sources and sinks is derived and the mean streamfunction is presented for the reanalysis data. The corresponding angular momentum budget is investigated in section 5. The conclusions and discussion are provided in section 6. Some detailed derivations are offered in the appendices.

2. Formulation of hybrid isobaric–isentropic diagnostics

a. Basic formulation

We first introduce the formulation of the diagnostics using the mass above isentropes as the vertical coordinate. This is equivalent to changing the vertical coordinate of the isentropic formulation from the potential temperature (e.g., Andrews 1983; Tung 1986) to the isentropic zonal-mean pressure (e.g., Iwasaki 1989, 1998; Tanaka et al. 2004). However, our formulation is derived from the pressure coordinate by treating entropy as a quasi-conservative tracer, analogous to the modified Lagrangian-mean formulation of Nakamura (1995) using a tracer as the meridional coordinate. The formulation can be readily generalized to moist entropy or other quasi-conservative tracers by construction.

Consider an instantaneous map of potential temperature in the longitude–pressure plane, as depicted in Fig. 1a. The temperature distribution does not have to be smooth or regular, and it can be strongly disturbed by extreme weather events such as intensive convection, Rossby wave breaking, or boundary layer mixing. As for the isentropic coordinate (e.g., Held and Schneider 1999), it would be convenient to define a density function σ by a Heaviside step function $\mathcal{H}(p_s - p)$ for the massless underground:

$$\sigma \equiv \mathcal{H}(p_s - p), \quad (1)$$

where p_s is the surface pressure, and the zonal mean $\bar{\sigma}(\phi, p, t)$ denotes the probability of the pressure surface p at the latitude ϕ and time t above the ground.

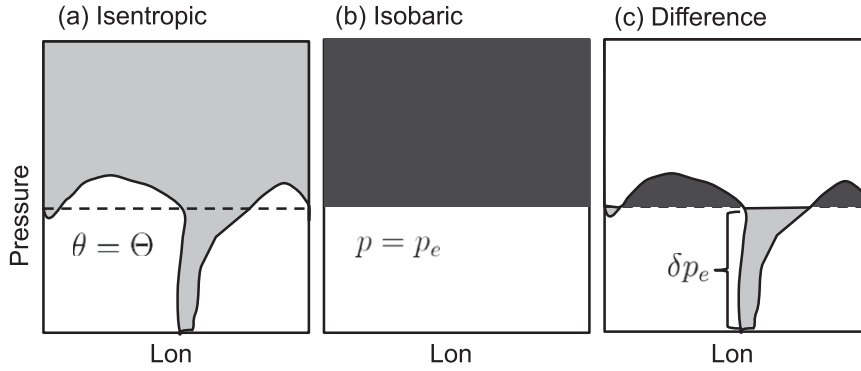


FIG. 1. Isentropic and isobaric area integrals with respect to the isentropes $\theta = \Theta$. The shading highlights (a) the area of integration for the isentropic area integral above $\theta = \Theta$ and (b) the isobaric integral above $p = p_e$. (c) The integral of the area in light shading minus the integral of area in dark shading. After a reversible (mass- and entropy-conserved) zonalization, the isentropic line Θ in (a) results in the isobar $p = p_e$ in (b), where the mass in light shading in (a) is equal to the mass in dark shading in (b). In (c), $\delta p_e(\lambda) = p(\lambda, \Theta) - p_e$ denotes the deviation of the mass and has zero zonal mean.

The mass above the isentropes $\theta = \Theta$ at ϕ and t (shading in Fig. 1a) can be written as

$$m(\phi, \Theta, t) = -\frac{a \cos \phi}{g} \int_{\theta > \Theta} d\theta \oint \sigma \left(\frac{\partial p}{\partial \theta} \right)_\theta d\lambda_\theta$$

$$= \frac{a \cos \phi}{g} \int_0^{p_s} \oint \sigma \mathcal{H}(\theta - \Theta) d\lambda dp, \quad (2)$$

where the first circuit integral is evaluated along the isentropic line: $d\lambda_\theta$ is the isentropic displacement in longitude and $(\partial p / \partial \theta)_\theta d\theta$ is the displacement in pressure normal to the isentropic line. The second circuit integral is evaluated along the isobaric line, the step function $\mathcal{H}(\theta - \Theta)$ ensures the mass above the isentropic surface Θ , and σ for the surface boundary condition.

Since potential temperature increases monotonically with height (i.e., positive static stability), the mass $m(\phi, \Theta, t)$ can be used to define a new vertical coordinate p_e —the pressure of the isentropic line after a reversible (mass- and entropy-conserved) zonalization (e.g., from Fig. 1a to Fig. 1b):

$$m(\phi, \Theta, t) = \frac{2\pi a \cos \phi}{g} \int_{p < p_e} \bar{\sigma} dp, \quad (3)$$

where p_e can be termed as the “ Θ -equivalent pressure,” analogous to the familiar concept of the equivalent latitude for the diagnostic of isentropic transport (Butchart and Remsberg 1986). At each latitude and time, this yields a one-to-one correspondence of $\Theta = \Theta[p_e(\Theta)]$ by

$$\left(\frac{\partial m}{\partial p_e} \right)_{\phi, t} = \frac{2\pi a \bar{\sigma} \cos \phi}{g}, \quad (4)$$

where the subscripts outside a bracket denote that the variable is held fixed when evaluating the partial derivation. In comparison with the isentropic zonal-mean pressure p_\uparrow , which is used as the vertical coordinate in the isentropic formulation of Iwasaki (1998), p_e is identical to p_\uparrow if the isentropic surface does not intersect the ground. But p_e can differ from p_\uparrow when the isentropic surface intersects the ground, as p_\uparrow does not include the step function σ in the formulation.

Next, for a quantity X , we can define the mass-weighted integral above the isentropic surface as (shading in Fig. 1a)

$$\mathcal{M}(X) = -\frac{a \cos \phi}{g} \int_{\theta > \Theta} d\theta \oint \sigma X \left(\frac{\partial p}{\partial \theta} \right)_\theta d\lambda_\theta$$

$$= \frac{a \cos \phi}{g} \int_0^{p_s} \oint \sigma X \mathcal{H}(\theta - \Theta) d\lambda dp. \quad (5)$$

Similar to the modified Lagrangian mean in Nakamura (1995), the isentropic mean can be defined as the mass-weighted average at the $\theta = \Theta$ contour:

$$\bar{X}^\Theta \equiv \left[\frac{\partial \mathcal{M}(X)}{\partial m} \right]_\Theta = \frac{\partial \mathcal{M}(X) / \partial \Theta}{\partial m / \partial \Theta}$$

$$= \oint_{\theta = \Theta} \sigma X \left(\frac{\partial p}{\partial \theta} \right)_\theta d\lambda_\theta / \oint_{\theta = \Theta} \sigma \left(\frac{\partial p}{\partial \theta} \right)_\theta d\lambda_\theta. \quad (6)$$

By definition, $\bar{\theta}^\Theta = \Theta$. Also, Θ is conserved in the absence of diabatic heating and diffusion. Since an isentropic surface can be regarded as a quasi-conservative material surface, \bar{X}^Θ can be seen as a quasi-Lagrangian mean of X . In practice, \bar{X}^Θ can be calculated by a finite-differencing scheme of $\mathcal{M}(X)$ with respect to m , and

therefore it is defined by quantities in the pressure coordinates.

Accordingly, by including σ , the isobaric mean can be written as the mass-weighted zonal mean at the pressure surface $p = p_e$ (Fig. 1b), and an eddy term can be defined as the deviation therefrom. If the pressure surface does not intersect the ground, they reduce to the regular zonal mean and eddy terms:

$$\begin{aligned}\bar{X}^p &= \frac{\sigma \bar{X}}{\bar{\sigma}} \\ X' &= X - \bar{X}^p.\end{aligned}\quad (7)$$

By this definition, $\bar{X}^p \equiv 0$, but \bar{X}' can be nonzero if the pressure surface intersects the ground.

Hereafter we set the pressure level in the isobaric mean \bar{X}^p equal to the equivalent pressure in the isentropic mean \bar{X}^{Θ} (i.e., $p = p_e$). For the isentropic mean, this results from a reversible (mass- and entropy-conserved) vertical adjustment of the isentropic line toward a zonally symmetric basic state, and p_e has a one-to-one correspondence to the mass above the isentrope Θ by Eq. (4). As such, we construct a hybrid isobaric–isentropic diagnostic using $p = p_e$ as the vertical coordinate.

b. Data and analysis method

In this study, we employ the National Centers for Environmental Prediction (NCEP)–U.S. Department of Energy (DOE) Reanalysis 2, an updated product of the NCEP–National Center for Atmospheric Research (NCAR) reanalysis (Kanamitsu et al. 2002). The data are available at the same resolution as the NCEP–NCAR reanalysis, with a $2.5^\circ \times 2.5^\circ$ horizontal resolution and 17 pressure levels. We analyze 6-hourly data for the period of 1979–2011, and the 6-hourly data are expected to capture the contributions of extreme weather events to the mass fluxes better than daily data.

To facilitate the vertical integral or derivative with respect to p or p_e , the meteorological fields are interpolated linearly onto 52 evenly spaced vertical levels from 20 to 1040 hPa with an increment of 20 hPa. By comparing the geopotential height with the surface orography, we determine whether a grid point is above or below the ground (i.e., the value of σ). Consistent with aforementioned formulation, the underground world is set as motionless (i.e., $u = v = \omega = 0$) and massless (i.e., $\sigma = 0$). In practice, to ensure a monotonic relationship between Θ and p_e in Eq. (4), we set a very small number for the mass density below the ground as $\sigma = 10^{-20}$, making it easier in coding than dealing with a constantly moving lower boundary. In terms of entropy, to be consistent with the isentropic coordinates in which

the underground mass density $-(1/g) \partial p / \partial \theta$ is zero, the underground potential temperature is interpolated downward by assuming a very large value of $\partial \theta / \partial p$.

Additionally, in computing the isentropic mass-weighted integral [i.e., Eqs. (2) and (5)] at a latitude and time, we first sort θ in an ascending order for all of the points. Then m and $\mathcal{M}(X)$ can be obtained for each value of Θ by aggregating all of the points with $\theta > \Theta$. The isentropic mean, defined by Eq. (6), is calculated by a finite-differencing scheme of $\mathcal{M}(X)$ with respect to m . Finally, the equivalent pressure [equivalently the mass above an isentrope by Eq. (4)] and the corresponding isentropic means are interpolated onto the same 52 pressure levels as the isobaric means to facilitate a hybrid isobaric–isentropic diagnostic.

We illustrate the usefulness of our diagnostic using the example of weather at 0000 UTC 28 December 2010. In Fig. 2a, the mean sea level pressure (MSLP) displays a notable extratropical storm at about 40°N , 60°W , known as the December 2010 North American blizzard. The longitude–pressure cross section of the storm at 40°N (Fig. 2b) displays a poleward (solid line) surface wind on the east of 60°W associated with warm air and an equatorward (dashed line) surface wind on the west associated with cold air. Similar poleward/warm-air and equatorward/cold-air correlations are evident elsewhere in the lower troposphere, as expected from the poleward heat transport by extratropical storms. In Figs. 2c–e, the isobaric means (black) and isentropic means (red) are compared. The isobaric zonal-mean meridional wind is characterized by an equatorward wind at 200 hPa and a poleward wind near the surface—a typical circulation pattern of the Ferrel cell. However, when averaging with respect to the isentropic surface and then transformed to the equivalent pressure, the mean meridional wind exhibits a poleward flow within 500–850 hPa and an equatorward flow below 850 hPa, where a fraction of pressure surface is underground, as indicated by $\sigma < 1$. This corresponds to the single overturning cell of the isentropic mean circulation. The two equivalent-pressure layers of 500–850 and 850–1000 hPa approximately correspond to the two isentropic layers of 290–310 and 270–290 K (Fig. 2e), and in Fig. 2b, the warmer layer portrays a Rossby wave pattern and the colder layer is seen to intersect the ground. Interestingly, the isentropic mean shows much colder temperature near the surface than the isobaric mean, which may be attributed to the cold temperature advection associated with the isentropic equatorward flow. In spite of the circulation diagnostic of a single day, the general pattern of mean meridional circulation in equivalent pressure agrees well with the mean circulation in the isentropic coordinate depicted in Held and Schneider (1999).

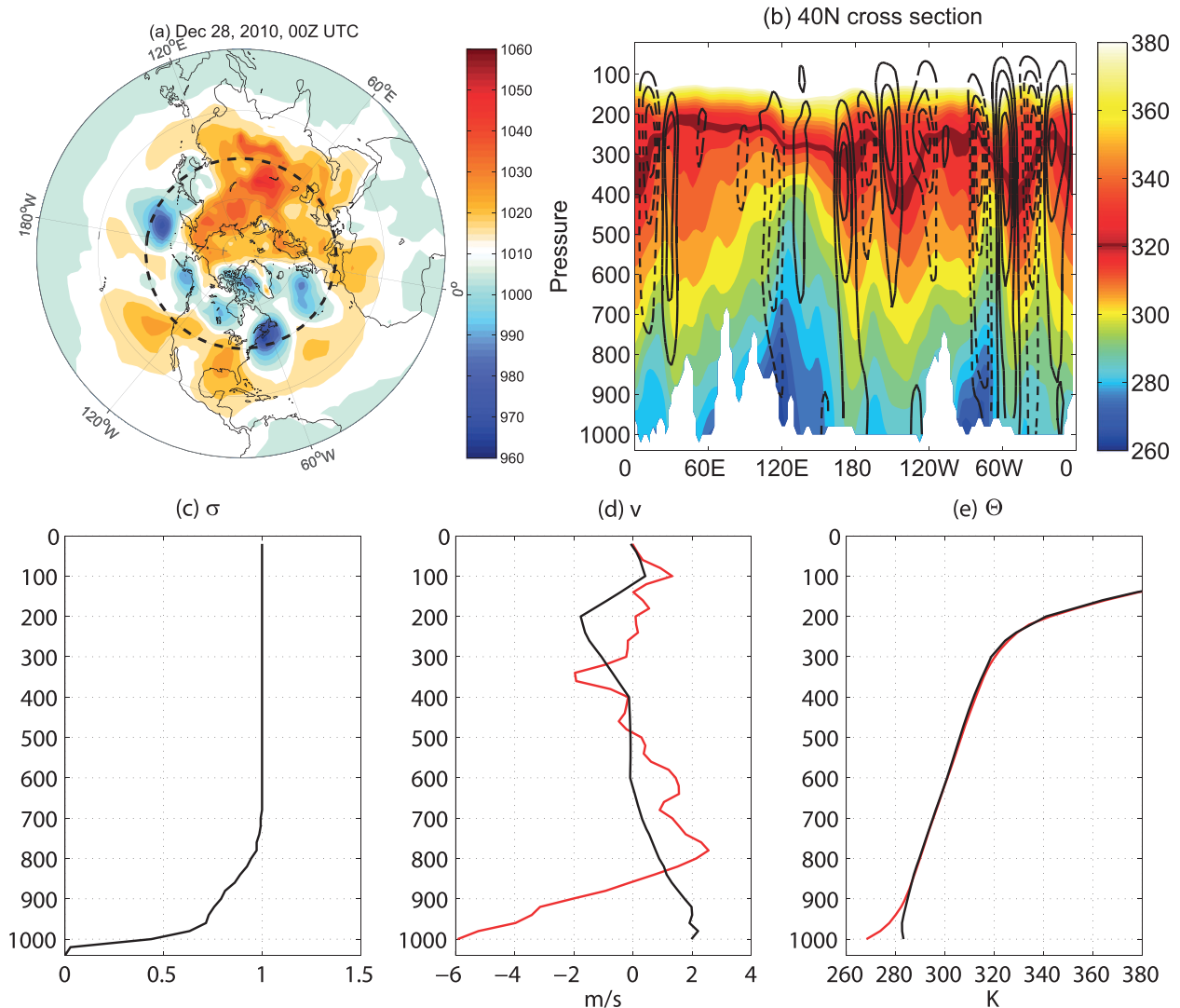


FIG. 2. An example of isobaric and isentropic mass-weighted means at 40°N at 0000 UTC 28 Dec 2010. (a) MSLP (hPa) is shown in shading, and the dashed line denotes 40°N. (b) The longitude–pressure cross section at 40°N, where the shading denotes potential temperature (K) and the contour denotes meridional wind (solid for positive, dashed for negative, and zero omitted; contour interval is 10 m s⁻¹). (c) The probability of pressure surface above the ground at 40°N, $\bar{\sigma}$. (d) Meridional wind, \bar{v}^{σ} and \bar{v}^{ρ} . (e) Potential temperature, $\bar{\Theta}$ and $\bar{\Theta}^{\rho}$. Black lines in (c)–(e) are isobaric zonal means and red lines are isentropic means. See Eqs. (6) and (7) for the definitions of notation.

3. Static stability and meridional wind

Here we discuss the isentropic static stability and meridional wind in comparison with their corresponding isobaric means, especially in the context of the near-surface stability and circulation. Figure 3 shows the isentropic mass-weighted mean potential temperature (dash-dotted) and the isentropic mean minus isobaric mean temperature (i.e., $\bar{\Theta} - \bar{\Theta}^{\rho}$, shown in solid and dashed lines) in December–February (DJF) and June–August (JJA) for the period 1979–2011. Similar to the circulation diagnostics of a single day in Fig. 2,

the time-averaged isentropic near-surface (where a fraction of pressure surface is below the ground, indicated by the light shading) temperature is colder than the isobaric mean, with a peak of about 11 K colder in the Northern Hemisphere (NH) winter, corresponding to about 1-K warming in the upper troposphere. The large contrast in warm and cold anomalies suggests that the surface cold extremes are very localized (i.e., small $\bar{\sigma}$), since the mass-weighted average of warm and cold anomalies at a latitude should be equal. Additionally, this suggests that the air mass in the isentropic coordinates is more stratified than the mass in the isobaric

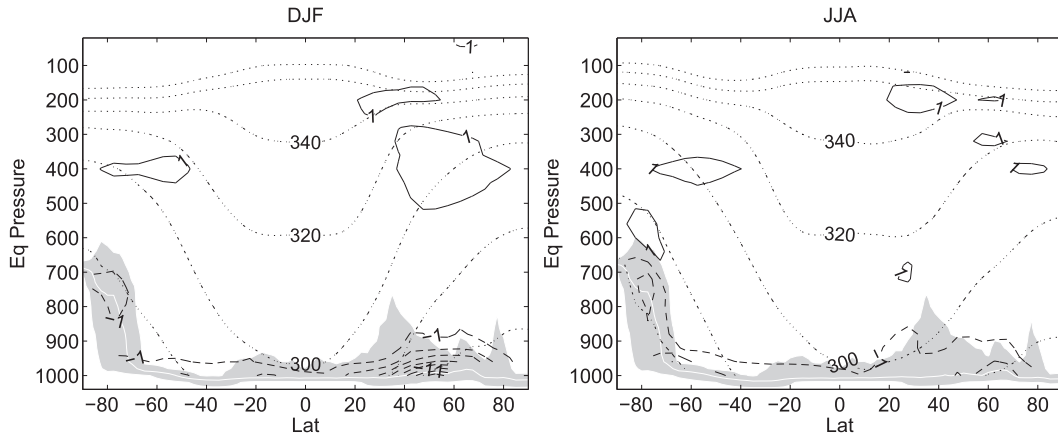


FIG. 3. Time and isentropic mass-weighted mean potential temperature (dash-dotted, contour interval is 20 K) and the difference between isentropic and isobaric means (i.e., $\Theta - \bar{\theta}^p$, solid for positive, dashed for negative; contour interval is 2 K) in (left) DJF and (right) JJA. Light shading indicates the pressure surface where the percentage of mass above the ground is between 10% and 90%.

coordinates, especially near the ground. These are consistent with Fig. 2b wherein there is more near-surface stratification over the colder air mass than over the warmer air mass.

Why is the air mass in the isentropic coordinates more stratified than the isobaric counterpart? We illustrate this using an idealized temperature profile with uniform stratification and a small-amplitude thermal perturbation. For a small-amplitude and conservative thermal perturbation, the temperature anomaly can be approximated as

$$\begin{aligned} \theta' &\approx -\delta\phi\partial\bar{\theta}^p/\partial\phi - \delta p\partial\bar{\theta}^p/\partial p \\ &= -\delta p \left[1 - \frac{(\partial p/\partial\phi)\bar{\theta}^p}{\delta p/\delta\phi} \right] \partial\bar{\theta}^p/\partial p, \end{aligned} \quad (8)$$

where $\delta\phi$ and δp denote the meridional and vertical parcel displacements, respectively. Figure 4 displays an idealized temperature profile with a wavenumber-1 perturbation, which may be attributed to either meridional and/or vertical parcel perturbation. The isentropic mass density, $-(1/g)(\partial p_e/\partial\Theta)$, gradually becomes zero

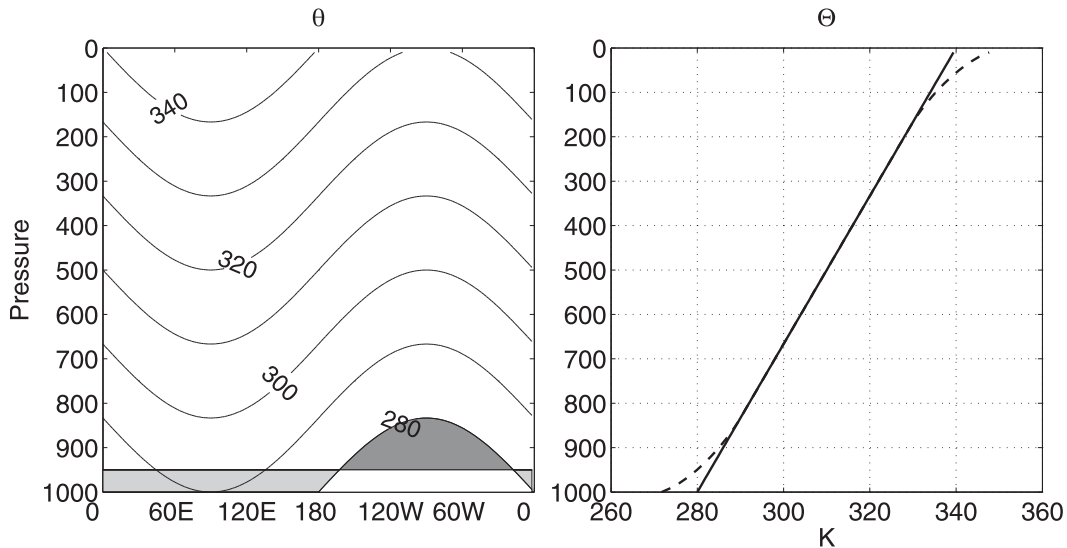


FIG. 4. (left) Idealized profile of potential temperature (K) with uniform stratification and a wavenumber-1 perturbation: $\theta(\lambda, p) = 280 + 60(1 - p/10^5) + 10 \sin(\lambda)$. The zonalization of the 280-K isentrope is denoted by shading as the area integral above the 280-K isentrope minus the integral above the corresponding $p_e \approx 950$ hPa, as exemplified in Fig. 1c. (right) The corresponding (solid) isobaric mean and (dashed) isentropic mean of the idealized temperature profile.

toward the surface, while the isobaric counterpart, $-(1/g)(\partial p/\partial \bar{\theta}^p)$, is a step function at the surface. As a result, the isobaric and isentropic mean static stability of this idealized profile are identical in the interior of the atmosphere, but the stratification with respect to isentropes, $-\partial \Theta/\partial p_e$, is larger than the isobaric counterpart, $-\partial \bar{\theta}^p/\partial p$, near the top and lower boundaries where the isentropic line intersects with the boundaries. If we think of the tropopause as the top boundary of tropospheric waves, this idealized example is consistent with Fig. 3 with positive $\Theta - \bar{\theta}^p$ in the upper troposphere and negative $\Theta - \bar{\theta}^p$ near the surface.

The increased stratification in the isentropic mean near the boundaries results from an entropy-conserved zonalization, which retains the extreme value of entropy, whereas the extreme value is smoothed in the zonal mean. For example, while the 280-K value in the zonal-mean temperature corresponds to the pressure level 1000 hPa, the reversible zonalization of the 280-K isentrope corresponds to the equivalent pressure $p_e \approx 950$ hPa. The reversible zonalization of the 280-K isentrope is demonstrated by the shading in Fig. 4 as the area integral above the 280-K isentrope minus the integral above the corresponding equivalent pressure 950 hPa. Interestingly, Eq. (8) becomes $\theta' \approx -\delta\phi(\partial \bar{\theta}^p/\partial \phi)$ at the ground, and therefore, the near-surface isentropic stratification is greater than the isobaric counterpart as the effect of the meridional mixing of surface entropy is included.

Next, to understand the isentropic mean meridional wind, we define an operator for the difference between the isentropic mass-weighted integral above Θ in Fig. 1a and the isobaric integral above $p = p_e$ in Fig. 1b, corresponding to the mass-weighted integral of light shading minus the integral of dark shading in Fig. 1c:

$$\begin{aligned} \Delta \mathcal{M}(X) &= \frac{g}{2\pi a \cos\phi} \left[\mathcal{M}(X) - \frac{a \cos\phi}{g} \int_{p < p_e} dp \oint \sigma X d\lambda \right] \\ &= \frac{1}{2\pi} \left(\iint_{\theta > \Theta, p < p_e} \sigma X d\lambda dp \right. \\ &\quad \left. - \iint_{\theta < \Theta, p > p_e} \sigma X d\lambda dp \right). \end{aligned} \tag{9}$$

By the definition of the equivalent pressure, $\Delta \mathcal{M}(1) = 0$ (i.e., the mass in light shading is equal to the mass in dark shading). Also, if Θ is zonally symmetric, the isentropic integral is equal to the isobaric integral, $\Delta \mathcal{M}(X) = 0$. Therefore, $\Delta \mathcal{M}(X)$ is an eddy quantity related to the thermal perturbation.

Applying the operator $\Delta \mathcal{M}$ to v , $\Delta \mathcal{M}(v)$ denotes an eddy quantity analogous to the wave activity defined in

Nakamura and Zhu (2010). As exemplified in Fig. 1c, high potential temperature in the light shading is carried poleward and low potential temperature in the dark shading is transported equatorward, and therefore, $\Delta \mathcal{M}(v)$ describes the poleward transport of heat. In the small-amplitude limit, it is related to eddy heat flux [derivations are shown in Eq. (A4)] by

$$\Delta \mathcal{M}(v) \approx -\frac{\overline{\sigma v' \theta'^p}}{\partial \Theta/\partial p_e}. \tag{10}$$

It is noteworthy that this is also a hybrid isobaric–isentropic formula, in which the static stability is evaluated normal to an isentropic surface rather than an isobaric surface, and the eddy flux is evaluated at constant pressure. Near the surface, $\partial p_e/\partial \Theta$ gradually approaches zero, and therefore $\Delta \mathcal{M}(v)$ is closed at the surface. Also as noted in appendix A, the small-amplitude form is not exact when the isentropic layer intersects the ground under the adiabatic condition. Diabatic heating or diffusion is expected near the ground in this case, as discussed in context of the diabatic surface layer in Plumb and Ferrari (2005).

Taking the derivative of Eq. (9) with respect to the mass m and using Eqs. (4), (6), and (7), one can obtain a simple relationship between the isentropic and isobaric mean meridional winds:

$$\bar{v}^\Theta - \bar{v}^p = \frac{1}{\bar{\sigma}} \frac{\partial \Delta \mathcal{M}(v)}{\partial p_e} \approx -\frac{1}{\bar{\sigma}} \frac{\partial}{\partial p_e} \left(\frac{\overline{\sigma v' \theta'^p}}{\partial \Theta/\partial p_e} \right), \tag{11}$$

where we have used the small-amplitude approximation in Eq. (10). In the interior of the atmosphere where $\sigma = 1$ and $\partial \Theta/\partial p_e \approx \partial \bar{\theta}^p/\partial p$, the isentropic mean meridional wind reduces to the residual meridional wind in the TEM framework (e.g., Andrews and McIntyre 1976; Edmon et al. 1980). Therefore, we see that $\Delta \mathcal{M}(v)$ is a finite-amplitude Stokes correction between the isobaric and isentropic mean winds.

We compare $\Delta \mathcal{M}(v)$ with its small-amplitude approximations in Fig. 5, using the isobaric and isentropic static stability, respectively, as the two differ near the ground. Similar to the seasonal cycle of eddy heat fluxes, $\Delta \mathcal{M}(v)$ is greatest in the winter hemispheres and smallest in the NH summer. Above the near-surface layer, as can be also inferred from the diagnostics of Tanaka et al. (2004), $\Delta \mathcal{M}(v)$ and its small-amplitude approximations agree very well, although using the isobaric static stability results in some subtle differences for the 6-hourly data we analyzed. As one moves into the near-surface layers, the formulations start to diverge. While σ leads to zero heat flux when the pressure surface is completely below the ground, the nearly neutral Eulerian static

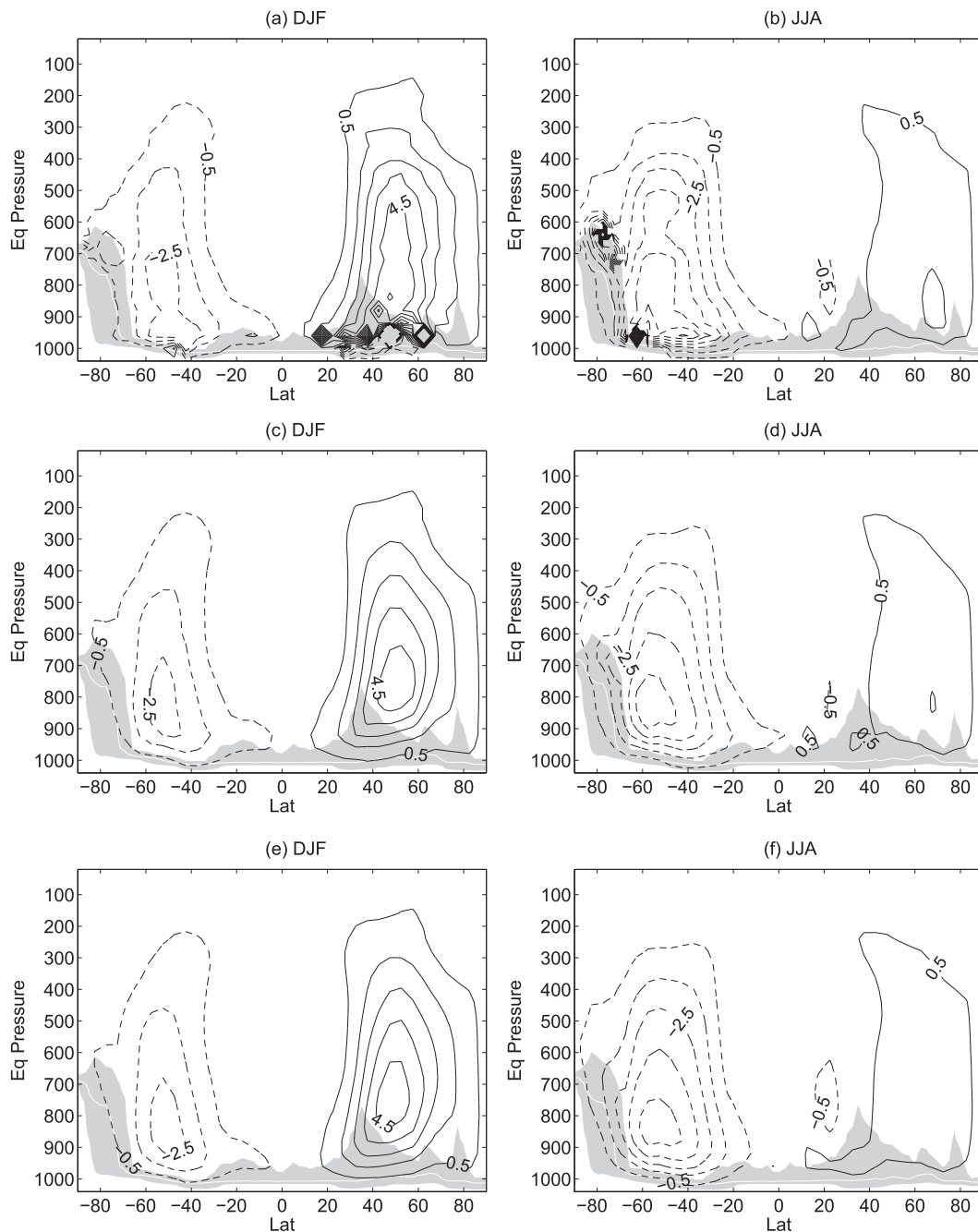


FIG. 5. A comparison of Stokes correction $\Delta\mathcal{M}(v)$ with its small-amplitude approximations in (left) DJF and (right) JJA. (a),(b) Isobaric means, $-\overline{\sigma v' \theta'^p} / (\partial \theta^p / \partial p)$. (c),(d) Isobaric mean eddy heat flux with isentropic static stability, $-\overline{\sigma v' \theta'^p} / (\partial \theta / \partial p_e)$. (e),(f) $\Delta\mathcal{M}(v)$. Contour intervals are $10^4 \text{ m s}^{-1} \text{ Pa}$. Light shading indicates the pressure surface where the percentage of mass above the ground is between 10% and 90%.

stability results in unrealistically large values of $-\overline{\sigma v' \theta'^p} / (\partial \theta^p / \partial p)$ near the surface, especially in the winter hemispheres. As pointed out by Held and Schneider (1999), the singularity in the near-surface isobaric static stability in the TEM formulation accounts for an unrealistically thin near-surface flow. Interestingly, this

shortcoming can be largely remedied by using the isentropic static stability. The isentropic static stability incorporates the effect of the meridional mixing in surface entropy, which is deemed crucial for the near-surface thermodynamical balance (e.g., Held and Schneider 1999; Plumb and Ferrari 2005). Despite the limitations

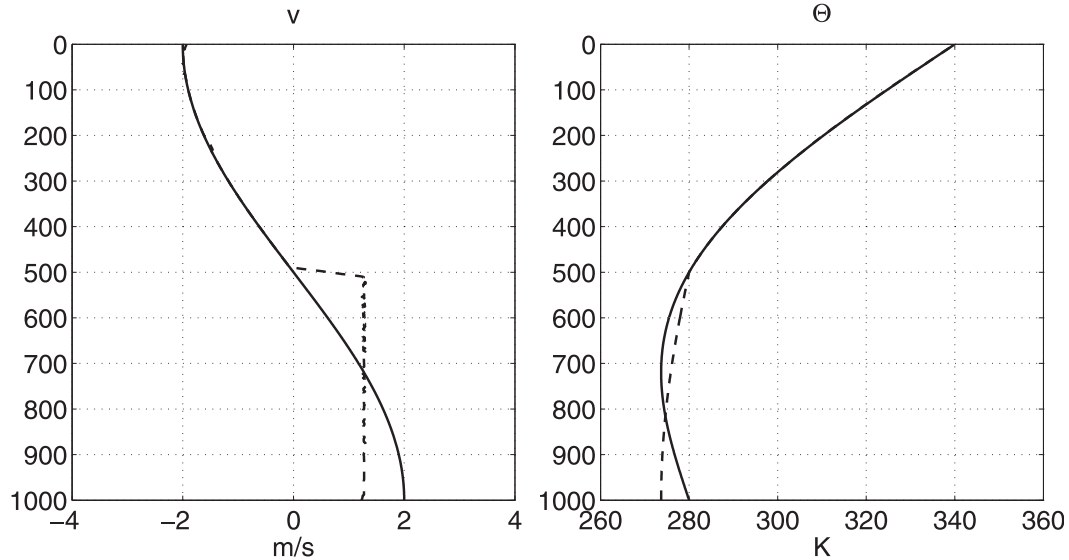


FIG. 6. Idealized zonally symmetric profiles of (left) meridional wind and (right) equivalent potential temperature as a function of pressure (hPa). The isobaric mean meridional wind is specified as $v(p) = -2\cos(\pi p/10^5)$ and equivalent potential temperature as $\theta_e(p) = 280 + 60(1 - p/10^5) - 30 \sin(\pi p/10^5)$, denoted by solid lines. The corresponding isentropic means are denoted by dashed lines.

of the small-amplitude form of Eq. (10), $-\overline{\sigma v \theta^p} / (\partial \Theta / \partial p_e)$ resembles the fully isentropic formulation well. Alternatively, the STEM formulation of Pauluis et al. (2011) resolves the near-surface problem by considering the Gaussian statistics. Our formulation deals with the near-surface problem by using the exact isentropic mean mass flux plus a formal transformation in the vertical coordinate, and it also shows the advantage of isentropic static stability for the near-surface flow over the isobaric static stability in the small-amplitude limit. As we will see later, this treatment also improves the mass streamfunction and EP flux for the near-surface flow. In the following sections, only the results with the finite-amplitude formulations are shown.

Also, $\Delta \mathcal{M}(v)$ can account for the meridional mass flux in a nonmonotonic vertical coordinate, in which it is more than an eddy term. As in Pauluis et al. (2008) and Pauluis et al. (2010), the mass streamfunction can be obtained by using the mass above moist isentropes as the vertical coordinate, and the magnitude of moist isentropic streamfunction is found to differ from dry isentropic streamfunction (not shown). Although our definitions in Eqs. (2) and (5) do not require the monotonicity of the vertical coordinate, the mean circulation in a nonmonotonic coordinate is more complex to interpret, as the change from the new coordinate p_e back to the geometric coordinate p is not a one-to-one correspondence.

For example, Fig. 6 depicts idealized zonally symmetric profiles of meridional wind and equivalent potential temperature, with a moist entropy minimum in

the lower troposphere. The isobaric means are denoted by solid lines and isentropic means by dashed lines. While there is no one-to-one correspondence from Θ to p because of the nonmonotonic profile, the correspondence from Θ to p_e can be established, as p_e corresponds to the total mass of the air parcel with the potential temperature larger than Θ in Eq. (2). In this idealized case, the isobaric mean static stability vanishes at the local minimum $\partial \theta^p / \partial p = 0$, but the isentropic mean $\partial \Theta / \partial p_e$ is nonzero by construction, as shown in the dashed line of Fig. 6. While the circulation is assumed zonally symmetric, the isentropic mean redistributes the meridional wind vertically, as a result of adjusting the nonmonotonic entropy profile to a monotonic basic state. In the small-amplitude form of Eq. (10), the eddy term would vanish. Therefore, the difference of the isentropic and isobaric means in this case does not represent an eddy term, but the zonally symmetric convective adjustment of the atmosphere. This is analogous to the discussion of wave activity associated with nonmonotonic zonally symmetric PV gradient in Fig. 3 of Nakamura and Zhu (2010). Despite the added complexity in interpretation, this demonstrates an advantage of the hybrid isobaric–isentropic formulation in understanding the mean circulation in nonmonotonic vertical coordinates.

4. Mean circulation and thermodynamic balance

In this section, we offer a rigorous derivation of Stokes correction in Eq. (11), its relationship to entropy sources

and sinks, and the static stability defined in the new coordinate. The thermodynamic energy equation in the pressure coordinate can be written in terms of potential temperature θ :

$$\frac{D\theta}{Dt} = \frac{\partial\theta}{\partial t} + \frac{v}{a} \frac{\partial\theta}{\partial\phi} + (u, \omega) \cdot \nabla_{\phi} \theta = \dot{\theta}, \quad (12)$$

where u , v , and ω are zonal, meridional, and pressure velocities; $\dot{\theta}$ is the source/sink of θ due to diabatic heating or turbulent diffusion; and ∇_{ϕ} is a gradient operator in the longitude–pressure plane defined as

$$\nabla_{\phi} = \left(\frac{1}{a \cos\phi} \frac{\partial}{\partial\lambda}, \frac{\partial}{\partial p} \right). \quad (13)$$

Considering the massless underground by the Heaviside step function σ , the continuity equation in the pressure coordinate can be written as¹

$$\frac{\partial\sigma}{\partial t} + \frac{1}{a \cos\phi} \frac{\partial(\sigma v \cos\phi)}{\partial\phi} + \nabla_{\phi} \cdot (\sigma u, \sigma \omega) = 0, \quad (14)$$

and the nondivergent streamfunction can be written as

$$\Psi = \frac{2\pi a \cos\phi}{g} \int_{p < p_e} \bar{\sigma} \bar{v}^p dp. \quad (15)$$

If all the air masses are above the ground (i.e., $\sigma \equiv 1$), the continuity equation and streamfunction reduce to their familiar isobaric forms (e.g., Holton 2004).

The mass budget above $\theta = \Theta$ in a longitude–pressure plane is illustrated in Fig. 7. The mass fluxes across an isentropic surface at a latitude are equal to the meridional fluxes above the same isentrope by mass continuity. Following Nakamura (1995) (the derivations are offered in appendix B), the continuity equation in the coordinates (ϕ, Θ, t) can be written as

$$\left(\frac{\partial m}{\partial t} \right)_{\phi, \Theta} + \frac{1}{a} \left[\frac{\partial \mathcal{M}(v)}{\partial \phi} \right]_{\Theta, t} + \left[\frac{\partial \mathcal{M}(\dot{\theta})}{\partial \Theta} \right]_{\phi, t} = 0. \quad (16)$$

Making the transformation in vertical coordinate from the potential temperature (ϕ, Θ, t) to the equivalent pressure (ϕ, p_e, t) ,

¹More generally, the continuity equation in the η (a monotonic function of pressure p) vertical coordinate on the sphere can be written as $(\partial/\partial t)(\partial p/\partial \eta) + (1/a \cos\phi)(\partial/\partial \lambda)[u(\partial p/\partial \eta)] + (1/a \cos\phi)(\partial/\partial \phi)[v(\partial p/\partial \eta) \cos\phi] + (\partial/\partial \eta)[\dot{\eta}(\partial p/\partial \eta)] = 0$ (Simmons and Burridge 1981). Here we set the mass density by the step function as $\partial p/\partial \eta = \sigma$.

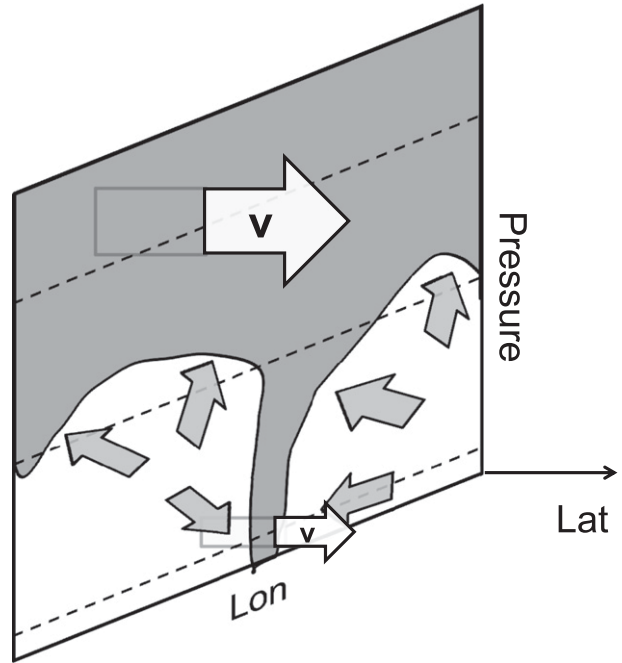


FIG. 7. The budget of mass above $\theta = \Theta$ at a latitude. Shaded arrows denote the mass fluxes across the Θ surface in the longitude–pressure plane and white arrows denote the corresponding mass fluxes across the latitude by mass continuity.

$$\begin{aligned} \left(\frac{\partial m}{\partial t} \right)_{\phi, \Theta} &= \left(\frac{\partial m}{\partial t} \right)_{\phi, p_e} - \left(\frac{\partial m}{\partial \Theta} \right)_{\phi, t} \left(\frac{\partial \Theta}{\partial t} \right)_{\phi, p_e} \\ \left[\frac{\partial \mathcal{M}(v)}{\partial \phi} \right]_{\Theta, t} &= \left[\frac{\partial \mathcal{M}(v)}{\partial \phi} \right]_{p_e, t} - \left[\frac{\partial \mathcal{M}(v)}{\partial \Theta} \right]_{\phi, t} \left(\frac{\partial \Theta}{\partial \phi} \right)_{p_e, t}. \end{aligned} \quad (17)$$

Substituting Eq. (17) into Eq. (16) and dividing by $-(\partial m/\partial \Theta)_{\phi, t}$ yields the thermodynamic energy equation in the coordinates (ϕ, p_e, t) :

$$\frac{D\Theta}{Dt} = \left(\frac{\partial \Theta}{\partial t} \right)_{\phi, p_e} + \frac{\bar{v}^{\Theta}}{a} \left(\frac{\partial \Theta}{\partial \phi} \right)_{p_e, t} + \bar{\omega}^e \left(\frac{\partial \Theta}{\partial p_e} \right)_{\phi, t} = \bar{\theta}^{-\Theta}, \quad (18)$$

where the mean meridional and vertical velocities in the coordinates (ϕ, p_e, t) are defined as

$$\begin{aligned} \bar{v}^{\Theta} &= \bar{v}^p + \frac{1}{\bar{\sigma}} \frac{\partial \Delta \mathcal{M}(v)}{\partial p_e} \\ \bar{\omega}^e &= \bar{\omega}^p - \frac{1}{a \bar{\sigma} \cos\phi} \frac{\partial [\Delta \mathcal{M}(v) \cos\phi]}{\partial \phi}. \end{aligned} \quad (19)$$

Here we have used Eqs. (4), (6), (7), and (9) (derivations are provided in appendix C). It is noteworthy that the mean vertical velocity in equivalent pressure $\bar{\omega}^e$ is not

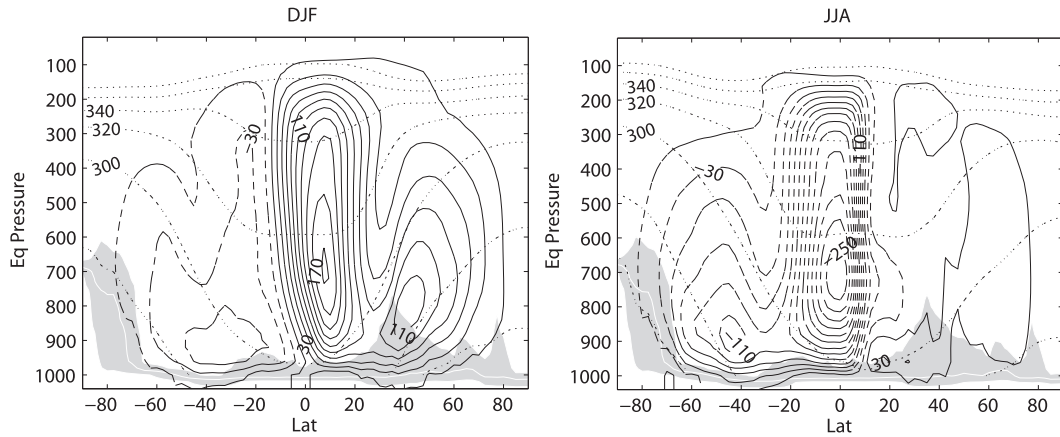


FIG. 8. Isentropic mass-weighted mean potential temperature (dash-dotted; contour interval is 20 K) and mass streamfunction (solid for positive and dashed for negative; contour interval is $20 \times 10^9 \text{ kg s}^{-1}$) in (left) DJF and (right) JJA. Light shading indicates the pressure surface where the percentage of mass above the ground is between 10% and 90%.

necessarily equal to the isentropic mean of the vertical velocity $\bar{\omega}^\Theta$ because of the change in vertical coordinate.

Equation (18) is an exact balance between the mean circulations in equivalent-pressure coordinates ($\bar{v}^\Theta, \bar{\omega}^\Theta$) and the entropy source/sink $\bar{\theta}^\Theta$. As Θ remains constant following the air parcel in absence of nonconservative processes, the mean circulations are the advecting velocities for the material derivative D/Dt in the (ϕ, p_e) plane. Since there is no eddy term in Eq. (18), the mean circulation is essentially equivalent to the isentropic circulation in Eq. (2.24) of Tanaka et al. (2004) in the interior of the atmosphere, which is derived by a change in vertical coordinate from the isentropic circulation of Andrews (1983).

From Eq. (C2), the corresponding continuity equation is

$$\left(\frac{\partial \bar{\sigma}}{\partial t}\right)_{\phi, p_e} + \left[\frac{1}{a \cos \phi} \frac{\partial (\bar{\sigma} \bar{v}^\Theta \cos \phi)}{\partial \phi}\right]_{p_e, t} + \left[\frac{\partial (\bar{\sigma} \bar{\omega}^\Theta)}{\partial p_e}\right]_{\phi, t} = 0. \tag{20}$$

In comparison with Eq. (2.19) of Tanaka et al. (2004), the probability density function $\bar{\sigma}$ is introduced in our formulation because of the inclusion of σ in the definition of p_e . The nondivergent mass streamfunction can be obtained by the vertical integral of the meridional mass flux from the top of the atmosphere to the Θ contour:

$$\begin{aligned} \Psi^\Theta &= \mathcal{M}(v) = \frac{2\pi a \cos \phi}{g} \int_0^{p_e} \bar{\sigma} \bar{v}^\Theta dp_e \\ &\approx \Psi - \frac{2\pi a \cos \phi}{g} \frac{\bar{\sigma} v \theta^{\text{TP}}}{\partial \Theta / \partial p_e}, \end{aligned} \tag{21}$$

where we have used Eq. (A4) for the small-amplitude approximation. Therefore, as discussed for Eq. (11), it is formally shown that Ψ^Θ is a finite-amplitude extension of the conventional TEM residual streamfunction (e.g., Andrews and McIntyre 1976; Edmon et al. 1980), and \bar{v}^Θ and $\bar{\omega}^\Theta$ in Eq. (19) are the corresponding extension of the residual velocities. As expected from Fig. 5, the conventional TEM works well where the isentropic surface does not intersect with the ground, where $\partial \Theta / \partial p_e \approx \partial \theta^{\text{TP}} / \partial p$ and $\sigma = 1$.

The mean mass streamfunction in equivalent pressure is displayed in Fig. 8 for DJF and JJA. As the TEM residual circulation (Edmon et al. 1980) or the isentropic mean circulation (e.g., Held and Schneider 1999; Tanaka et al. 2004), there exists a single-cell circulation in each hemisphere. The tropical circulation describes a solstitial Hadley cell circulation, characterized by an intense updraft within 10° latitude of the summer hemisphere, crossing the equator in the upper troposphere, and then descending in the subtropics of the winter hemisphere. The intensity² of tropical circulation is stronger in JJA than DJF, possibly owing to larger diabatic heating associated with the monsoons in the NH. The extratropical circulation rises approximately along the isentropic surface, for example, moving along the 300-K isentropic surface from the subtropical lower troposphere to extratropical upper troposphere. This suggests that the entropy source/sink in Eq. (18) is

² One should note a difference in magnitude between this study and Fig. 1 of Tanaka et al. (2004). This is due to the difference between the NCEP-NCAR and NCEP-DOE reanalyses (cf. Stachnik and Schumacher 2011).

secondary in the extratropical middle-to-upper troposphere. The intensity of extratropical circulation peaks at a similar magnitude in both winter hemispheres, and the intensity is weakest in the NH summer because of weak baroclinic eddies (cf. the heat fluxes in Fig. 5). The high-latitude subsidence moves equatorward near the surface where the isentropes intersect the ground, completing the mean circulation within a finite-depth near-surface layer. These circulation patterns agree well with those in the isentropic coordinates.

As in Tanaka et al. (2004), the key distinction of our hybrid isobaric–isentropic diagnostics from the isentropic diagnostics lies in that the time or latitudinal integral/derivative is evaluated at the surface of constant mass rather than constant entropy, although the zonal average is both calculated on constant potential temperature surface. When using mass as the vertical coordinate, the majority of air mass lies above the mean surface pressure; it is then a more convenient coordinate to visualize the mean circulation than the isentropic coordinate.

5. Angular momentum balance and Eliassen–Palm flux

Previous studies investigated the angular momentum balance near the surface in the isentropic coordinates (e.g., Held and Schneider 1999; Koh and Plumb 2004; Schneider 2005) and geometric coordinates (Plumb and Ferrari 2005; Kuo et al. 2005). Here we present the angular momentum budget with the hybrid isobaric–isentropic framework, similar to Iwasaki (1998). Considering the boundary condition, the zonal-mean momentum budget of the atmosphere in the pressure coordinates can be written as

$$\begin{aligned} \frac{\partial \bar{u}^p}{\partial t} - \bar{v}^p (f + \bar{\zeta}^p) + \bar{\omega}^p \frac{\partial \bar{u}^p}{\partial p} \\ = -\frac{1}{a\bar{\sigma} \cos^2 \phi} \frac{\partial (\bar{\sigma} \bar{v}' u'^p \cos^2 \phi)}{\partial \phi} - \frac{1}{\bar{\sigma}} \frac{\partial (\bar{\sigma} \bar{\omega}' u'^p)}{\partial p} + \bar{N}^p, \end{aligned} \quad (22)$$

where N denotes the surface friction and other momentum source/sink. The absolute vorticity $f + \bar{\zeta}^p$ is related to zonal-mean angular momentum $\mathbf{M} = a \cos \phi (\bar{u}^p + \Omega a \cos \phi)$ by

$$f + \bar{\zeta}^p = -\frac{1}{a^2 \cos \phi} \frac{\partial \mathbf{M}}{\partial \phi}. \quad (23)$$

As in the TEM framework, we can replace the isobaric advecting winds by the mean circulations in equivalent pressure, and then construct the material derivative of the angular momentum in the latitude–equivalent pressure plane as

$$\frac{1}{a \cos \phi} \frac{D\mathbf{M}}{Dt} = \frac{\partial \bar{u}^p}{\partial t} - \bar{v}^\Theta (f + \bar{\zeta}^p) + \bar{\omega}^e \frac{\partial \bar{u}^p}{\partial p} = \nabla \cdot \mathbf{F} + \bar{N}^p. \quad (24)$$

It is shown in appendix C that the EP flux divergence in this hybrid framework can be written as

$$\begin{aligned} \nabla \cdot \mathbf{F} = & -\frac{1}{a\bar{\sigma} \cos^2 \phi} \frac{\partial}{\partial \phi} \left\{ \left[\bar{\sigma} \bar{v}' u'^p + \frac{\partial \bar{u}^p}{\partial p} \Delta \mathcal{M}(v) \right] \cos^2 \phi \right\} \\ & - \frac{1}{\bar{\sigma}} \frac{\partial}{\partial p} \left[\bar{\sigma} \bar{\omega}' u'^p + (f + \bar{\zeta}^p) \Delta \mathcal{M}(v) \right]. \end{aligned} \quad (25)$$

Note that this is a hybrid isobaric–isentropic diagnostic: the eddy momentum fluxes and wind shears are calculated from the isobaric means, but $\Delta \mathcal{M}(v)$, an eddy quantity related to eddy heat fluxes, is calculated from the difference between the isentropic and isobaric means.

From Eqs. (18) and (24), we see that both the mean circulation and the EP flux divergence would vanish for adiabatic and frictionless flow in the steady state. This is the nonacceleration theorem of finite-amplitude non-geostrophic eddies on the sphere analogous to the isentropic counterpart (Andrews 1983; Iwasaki 1998) or the geometric counterpart (Plumb and Ferrari 2005). Compared with the isentropic formulation [Eq. (5) in Iwasaki 1998], Eq. (24) describes the variability of the isobaric zonal wind \bar{u}^p rather than the isentropic mean wind \bar{u}^Θ . The EP flux has a straightforward connection to the TEM formulation, and it is much simpler than Eqs. (2.14) and (2.15) of Tanaka et al. (2004), which require additional knowledge of diabatic heating. Using Eq. (A4), the small-amplitude limit of Eq. (25) yields

$$\begin{aligned} \nabla \cdot \mathbf{F} \approx & -\frac{1}{a\bar{\sigma} \cos^2 \phi} \frac{\partial}{\partial \phi} \left[\bar{\sigma} \left(\bar{v}' u'^p - \frac{\partial \bar{u}^p}{\partial p} \frac{\bar{v}' \theta'^p}{\partial \Theta / \partial p_e} \right) \cos^2 \phi \right] \\ & - \frac{1}{\bar{\sigma}} \frac{\partial}{\partial p} \left\{ \bar{\sigma} \left[\bar{\omega}' u'^p - (f + \bar{\zeta}^p) \frac{\bar{v}' \theta'^p}{\partial \Theta / \partial p_e} \right] \right\}. \end{aligned} \quad (26)$$

In the interior of the atmosphere where $\sigma = 1$ and $\partial \Theta / \partial p_e \approx \partial \theta^p / \partial p$, this reduces to the familiar TEM EP flux divergence (e.g., Andrews et al. 1987). Near the surface, this seems to be a better approximation of Eq. (25) as the isentropic static stability incorporates the effect of meridional mixing of surface temperature. Compared with the formulation of Plumb and Ferrari (2005), this formulation appears to be simpler, but it is expressed in term of the isentropic static stability that is nonlocal in the geometric coordinates.

The angular momentum balance is presented for the reanalysis in DJF and JJA (Fig. 9). The EP flux

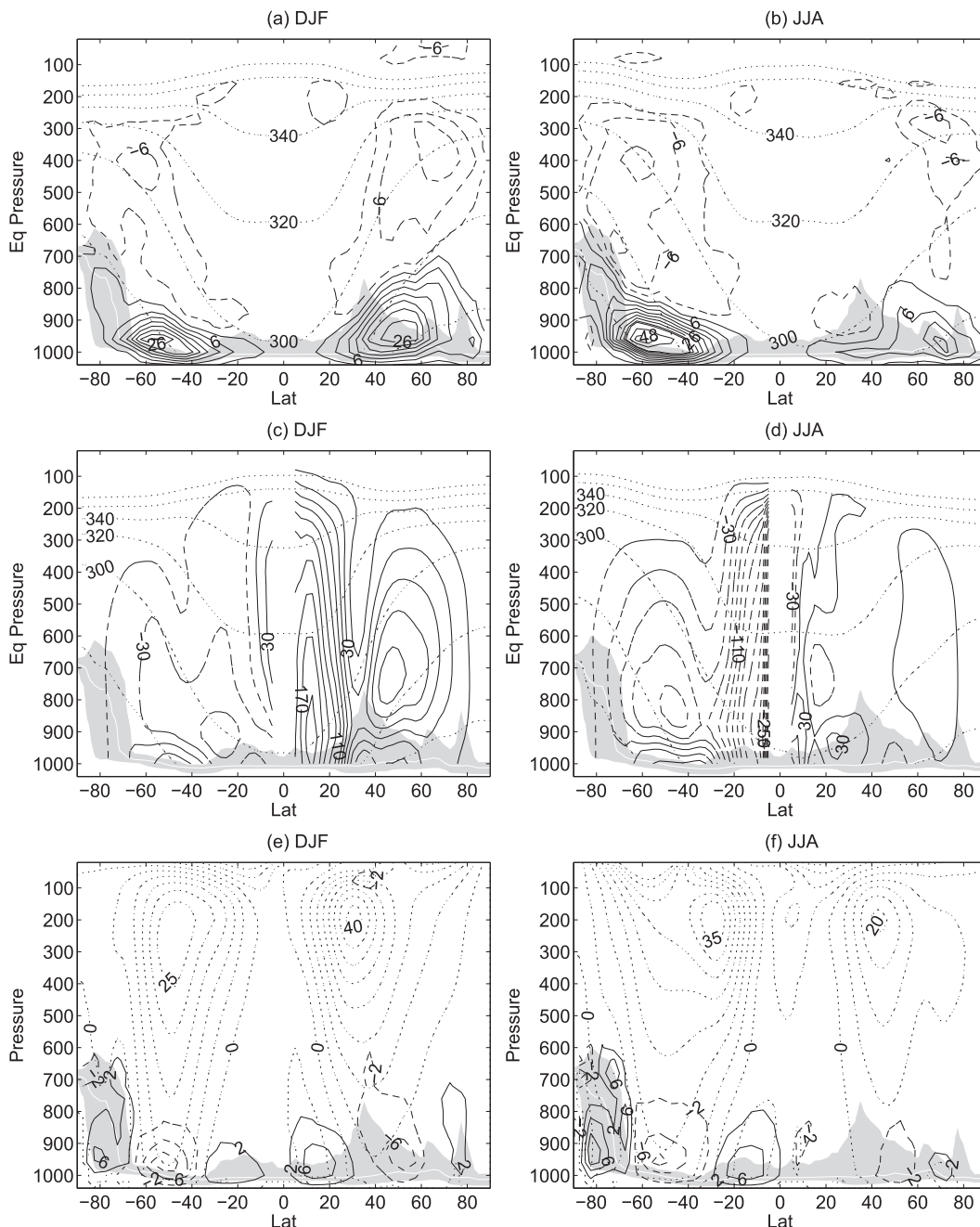


FIG. 9. The angular momentum balance in (left) DJF and (right) JJA. (a),(b) Isentropic mass-weighted mean potential temperature (dash-dotted; contour interval is 20 K) and EP flux divergence (solid for positive and dashed for negative; contour interval is $4 \text{ m s}^{-1} \text{ day}^{-1}$ and, for values larger than $30 \text{ m s}^{-1} \text{ day}^{-1}$, is $8 \text{ m s}^{-1} \text{ day}^{-1}$). (c),(d) As in Fig. 8, but for potential temperature and mass streamfunction diagnosed from the EP flux divergence. (e),(f) Zonal-mean zonal wind (dash-dotted; contour interval is 5 m s^{-1}) and the residual of angular momentum balance (solid for positive and dashed for negative; contour interval is $4 \text{ m s}^{-1} \text{ day}^{-1}$). Both the EP flux divergence and residual are multiplied by $\bar{\sigma}$. Light shading indicates the pressure surface where the percentage of mass above the ground is between 10% and 90%.

divergence is mostly confined in the near-surface layers, and the corresponding convergence lies within the isentropic layers aloft. As the EP flux convergence in the interior of the atmosphere reduces to the TEM

formulation in the small-amplitude limit, it may be regarded as a finite-amplitude extension of the PV flux. The EP flux convergence aloft aligns approximately along the isentropic surfaces, which can be thought of

as the result of the isentropic mixing of PV, analogous to the isentropic mixing of passive tracers found in geometric coordinates (e.g., Plumb and Mahlman 1987). As the EP flux divergence and convergence largely cancel each other in the mass-weighted vertical average, their magnitudes must be inversely proportional to their masses. Indeed, the ratio of the divergence versus convergence is about a factor of 4–5 in the SH and 2–3 in the NH, and this is consistent the ratio of masses between the free troposphere and near-surface layers.

As the meridional gradient of angular momentum is much larger than its vertical gradient, ignoring the vertical angular momentum transport and momentum source \bar{N}^p in Eq. (24), the meridional mass flux can be obtained from the EP flux divergence as the downward control diagnostic (Haynes et al. 1991)

$$\Psi^\Theta \approx -\frac{2\pi a \cos\phi}{g} \int_0^{p_e} \frac{\bar{\sigma}}{f + \bar{\zeta}^p} (\mathbf{V} \cdot \mathbf{F}) dp_e. \quad (27)$$

Figures 9c and 9d show the mass streamfunction diagnosed from the EP flux divergence from the angular momentum balance above. It agrees well with the mass streamfunction calculated directly except in the deep tropics and near-surface layer (cf. Figs. 8 and 9). In the deep tropics, the downward control diagnostic breaks down, since $f + \bar{\zeta}^p \approx 0$. The diagnosed streamfunction is not closed near the surface, as expected from the surface friction as momentum sources/sinks. To show this, the residual of the angular momentum balance is presented in the Figs. 9e and 9f. The residual displays a westward deceleration at the latitudes of surface westerlies and an eastward acceleration at the latitudes of surface easterlies; both are consistent with the expected surface friction. The residual-based friction is opposite in sign to the EP flux divergence at the latitudes of westerlies, and the magnitude of friction is about $1/3$ – $1/5$ of the EP flux divergence. Additionally, another region of significant residual is above the subtropical jet in the NH winter, and this can be attributed to the small-scale orographic gravity wave drag. Overall, the dominance of the EP flux divergence in the mass streamfunction highlights the critical role of isentropic mixing of potential vorticity in determining the mean mass transport circulation from the subtropics to the poles.

6. Conclusions and discussion

In this paper, we present the mean meridional circulation of the atmosphere using the mass above the isentropes of interest as the vertical coordinate. In this vertical coordinate, the mass-weighted mean circulation is exactly

balanced by entropy sources and sinks with no eddy flux contribution as in the isentropic coordinate (e.g., Andrews 1983; Tung 1986; Iwasaki 1998), and the coordinate can be readily generalized to the mass above moist isentropes or other quasi-conservative tracers, as in the tracer-based coordinate in the modified Lagrangian-mean diagnostic of Nakamura (1995). We also illustrate the applicability of this framework to an idealized nonmonotonic moist entropy profile, and it would be interesting to apply this diagnostic to the mean circulation in the moist isentropic coordinates of Pauluis et al. (2008, 2010). The new framework here is not restricted by the Gaussian statistics assumed by Pauluis et al. (2011) in dealing with nonmonotonic vertical coordinates.

It is shown in the NCEP–DOE Reanalysis 2 that the new formulation resolves the deficiency of the conventional TEM formulation for the near-surface flow as well as converges to the conventional TEM in the free troposphere. In the small-amplitude limit, the hybrid isobaric–isentropic formulation reduces to the TEM formulation. Therefore, the key improvement near the surface can be partially attributed to the isentropic static stability [the isentropic mass density $-(1/g)(\partial p_e/\partial \Theta)$ and Stokes correction in the small-amplitude limit in Eq. (10) gradually approach zero at the surface], which incorporates the effect of meridional eddy heat flux at the surface. This is consistent with Held and Schneider (1999) and Plumb and Ferrari (2005), who emphasize the effect of near-surface meridional temperature mixing in the thermodynamic balance.

The corresponding EP flux divergence for the zonal-mean angular momentum is formulated in a hybrid isobaric–isentropic form, extending the conventional TEM formulation (Andrews and McIntyre 1976; Edmon et al. 1980) to finite-amplitude nongeostrophic eddies on the sphere. This has a straightforward connection to the TEM counterpart in comparison with the isentropic formulation (Andrews 1983; Iwasaki 1998) or the geometric counterpart (Plumb and Ferrari 2005). Following the downward control diagnostic of Haynes et al. (1991), the mean mass streamfunction can be approximately obtained from the EP flux divergence except for the deep tropics or the near-surface flow, highlighting the dominant control of potential vorticity mixing for the subtropics-to-pole mean circulations. It is then expected to provide a valuable diagnostic framework not only for global circulation theory but also for atmospheric transport in the troposphere.

Acknowledgments. I thank Alan Plumb and Noboru Nakamura for valuable discussions throughout this work. I am also grateful for Olivier Pauluis and anonymous reviewers whose comments led to substantial

improvements of the manuscript. The author is supported by the National Science Foundation (NSF) Climate and Large-Scale Dynamics program under Grants AGS-1042787 and AGS-1064079.

APPENDIX A

Small-Amplitude Limit of $\Delta\mathcal{M}(v)$

Consider a small-amplitude thermal perturbation with the isentrope Θ disturbed from the pressure level p_e by a small displacement $\delta p_e(\lambda) = p(\lambda, \Theta) - p_e$, where $p(\lambda, \Theta)$ is the pressure at Θ , as illustrated by Fig. 1. The isentropic line can intersect the ground or not. For a conservative perturbation, the temperature anomaly can be approximated as

$$\theta' \equiv \theta - \bar{\theta}^p \approx -\delta p_e \frac{\partial \Theta}{\partial p_e}. \quad (\text{A1})$$

From the definition of the equivalent pressure, the mass above Θ and the mass above p_e are equal. Using Eq. (9), we have

$$\overline{\sigma \delta p_e} \approx \overline{\int_{p_e}^{p_e + \delta p_e(\lambda)} \sigma dp} = \Delta\mathcal{M}(1) = 0. \quad (\text{A2})$$

The operator $\Delta\mathcal{M}(v)$ in Eq. (9) can be written as

$$\Delta\mathcal{M}(v) = \overline{\int_{p_e}^{p_e + \delta p_e(\lambda)} \sigma v dp}. \quad (\text{A3})$$

Using Eq. (A2) and $v = v' + \bar{v}^p$, one obtains

$$\begin{aligned} \Delta\mathcal{M}(v) &\approx \overline{\int_{p_e}^{p_e + \delta p_e(\lambda)} \sigma v' dp} + \bar{v}^p \overline{\int_{p_e}^{p_e + \delta p_e(\lambda)} \sigma dp} \\ &\approx \overline{\sigma v' \delta p_e} = -\frac{\overline{\sigma v' \theta'^p}}{\partial \Theta / \partial p_e}, \end{aligned} \quad (\text{A4})$$

and we have substituted with Eq. (A1) in the final equality. We see that $\Delta\mathcal{M}(v)$ is proportional to the eddy heat flux divided by the isentropic static stability parameter in the small-amplitude limit. In this formula, the static stability is evaluated normal to an isentropic surface rather than an isobaric surface, but the eddy flux is evaluated at constant pressure. The difference between the isentropic and isobaric static stability is discussed in section 3.

It should be noted that the approximation in Eq. (A1) is not exact when the isentropic surface intersects the ground under the adiabatic condition. For example, in the left panel of Fig. 4, δp_e is constant for most of the

light-shaded area, and therefore Eq. (A1) is insufficient to describe the temperature anomaly. Diabatic heating or diffusion is expected in this case, as discussed in context of the diabatic surface layer in Plumb and Ferrari (2005).

APPENDIX B

Continuity Equation [Eq. (16)]

The continuity equation can be obtained by following the derivations in the appendix of Nakamura (1995). Nakamura (1995) used the coordinates (Q, θ, t) , where Q is a tracer for the meridional coordinate and $\dot{\theta}$ is the vertical velocity. Here we use the coordinates (ϕ, Θ, t) , where the potential temperature Θ is for the vertical coordinate and v is the meridional velocity. The rate of change in mass above the Θ isentrope at a fixed latitude and time is

$$\begin{aligned} \frac{\partial m(\phi, \Theta, t)}{\partial t} &= \frac{a \cos \phi}{g} \frac{\partial}{\partial t} \iint_{\theta > \Theta} \sigma d\lambda dp \\ &= \frac{a \cos \phi}{g} \iint_{\theta > \Theta} \frac{\partial \sigma}{\partial t} d\lambda dp - \frac{a \cos \phi}{g} \frac{\partial}{\partial \Theta} \iint_{\theta > \Theta} \sigma \frac{\partial \theta}{\partial t} d\lambda dp \\ &= \frac{a \cos \phi}{g} \frac{\partial}{\partial \Theta} \left[\Theta \iint_{\theta > \Theta} \frac{\partial \sigma}{\partial t} d\lambda dp - \iint_{\theta > \Theta} \frac{\partial(\sigma \theta)}{\partial t} d\lambda dp \right]. \end{aligned} \quad (\text{B1})$$

Equations (12) and (14) give the flux form of continuity and thermodynamic equations

$$\begin{aligned} \frac{\partial \sigma}{\partial t} &= -\frac{1}{a \cos \phi} \frac{\partial(\sigma v \cos \phi)}{\partial \phi} - \nabla_\phi \cdot (\sigma u, \sigma \omega) \\ \frac{\partial(\sigma \theta)}{\partial t} &= -\frac{1}{a \cos \phi} \frac{\partial(\sigma v \theta \cos \phi)}{\partial \phi} - \nabla_\phi \cdot (\sigma u \theta, \sigma \omega \theta) + \sigma \dot{\theta}. \end{aligned} \quad (\text{B2})$$

Substituting into Eq. (B1) and using the divergence theorem, and noting the identity

$$\begin{aligned} &\frac{1}{a \cos \phi} \frac{\partial}{\partial \phi} \iint_{\theta > \Theta} \sigma v \cos \phi d\lambda dp \\ &= \frac{1}{a \cos \phi} \left[\iint_{\theta > \Theta} \frac{\partial(\sigma v \cos \phi)}{\partial \phi} d\lambda dp \right. \\ &\quad \left. - \frac{\partial}{\partial \Theta} \iint_{\theta > \Theta} \sigma v \cos \phi \frac{\partial \theta}{\partial \phi} d\lambda dp \right], \end{aligned} \quad (\text{B3})$$

one obtains the continuity equation in the (ϕ, Θ, t) coordinates

$$\begin{aligned} \frac{\partial m}{\partial t} &= -\frac{a \cos \phi}{g} \frac{\partial}{\partial \Theta} \iint_{\theta > \Theta} \sigma \dot{\theta} d\lambda dp \\ &\quad - \frac{1}{a} \frac{\partial}{\partial \phi} \left(\frac{a \cos \phi}{g} \iint_{\theta > \Theta} \sigma v d\lambda dp \right) \\ &= -\frac{\partial \mathcal{M}(\dot{\theta})}{\partial \Theta} - \frac{1}{a} \frac{\partial \mathcal{M}(v)}{\partial \phi}. \end{aligned} \quad (\text{B4})$$

APPENDIX C

Mean Circulation in Equivalent Pressure [Eq. (19)] and Eliassen–Palm Flux [Eq. (25)]

Using Eqs. (14) and (15), and the definitions of Eqs. (4) and (7), the isobaric mean meridional and vertical winds can be written in terms of the non-divergent streamfunction

$$\begin{aligned} \bar{v}^p &= \frac{g}{2\pi a \bar{\sigma} \cos \phi} \left(\frac{\partial \Psi}{\partial p} \right)_{\phi, t} \\ \bar{\omega}^p &= -\frac{g}{2\pi a \bar{\sigma} \cos \phi} \left[\frac{1}{a} \left(\frac{\partial \Psi}{\partial \phi} \right)_{p, t} + \left(\frac{\partial m}{\partial t} \right)_{\phi, p} \right]. \end{aligned} \quad (\text{C1})$$

From Eqs. (16), (17), and (18), and the definitions of Eqs. (4) and (6), one can obtain the mean meridional and vertical winds in equivalent pressure:

$$\begin{aligned} \bar{v}^\theta &= \frac{g}{2\pi a \bar{\sigma} \cos \phi} \left[\frac{\partial \mathcal{M}(v)}{\partial p_e} \right]_{\phi, t} \\ \bar{\omega}^e &= -\frac{g}{2\pi a \bar{\sigma} \cos \phi} \left\{ \frac{1}{a} \left[\frac{\partial \mathcal{M}(v)}{\partial \phi} \right]_{p_e, t} + \left(\frac{\partial m}{\partial t} \right)_{\phi, p_e} \right\}. \end{aligned} \quad (\text{C2})$$

Using the definition (9), the hybrid isobaric–isentropic diagnostic (i.e., $p = p_e$) yields the mean circulation with Stokes correction in Eq. (19):

$$\begin{aligned} \bar{v}^\theta &= \bar{v}^p + \frac{1}{\bar{\sigma}} \frac{\partial \Delta \mathcal{M}(v)}{\partial p_e} \\ \bar{\omega}^e &= \bar{\omega}^p - \frac{1}{a \bar{\sigma} \cos \phi} \frac{\partial [\Delta \mathcal{M}(v) \cos \phi]}{\partial \phi}. \end{aligned} \quad (\text{C3})$$

Next, the difference of Eqs. (22) and (24) gives

$$\begin{aligned} \mathbf{V} \cdot \mathbf{F} &= -\frac{1}{a \bar{\sigma} \cos^2 \phi} \frac{\partial (\bar{\sigma} \bar{v} \bar{u}^p \cos^2 \phi)}{\partial \phi} - \frac{1}{\bar{\sigma}} \frac{\partial (\bar{\sigma} \bar{\omega} \bar{u}^p)}{\partial p} \\ &\quad - (\bar{v}^\theta - \bar{v}^p)(f + \bar{\zeta}^p) + (\bar{\omega}^e - \bar{\omega}^p) \frac{\partial \bar{u}^p}{\partial p}. \end{aligned} \quad (\text{C4})$$

Substituting Eq. (C3) into Eq. (C4) and using $p = p_e$, one obtains the EP flux divergence in the hybrid diagnostic framework

$$\begin{aligned} \mathbf{V} \cdot \mathbf{F} &= -\frac{1}{a \bar{\sigma} \cos^2 \phi} \frac{\partial}{\partial \phi} \left\{ \left[\bar{\sigma} \bar{v} \bar{u}^p + \frac{\partial \bar{u}^p}{\partial p} \Delta \mathcal{M}(v) \right] \cos^2 \phi \right\} \\ &\quad - \frac{1}{\bar{\sigma}} \frac{\partial}{\partial p} \left[\bar{\sigma} \bar{\omega} \bar{u}^p + (f + \bar{\zeta}^p) \Delta \mathcal{M}(v) \right]. \end{aligned} \quad (\text{C5})$$

REFERENCES

- Andrews, D. G., 1983: A finite-amplitude Eliassen–Palm theorem in isentropic coordinates. *J. Atmos. Sci.*, **40**, 1877–1883.
- , and M. E. McIntyre, 1976: Planetary waves in horizontal and vertical shear: The generalized Eliassen–Palm relation and the mean zonal acceleration. *J. Atmos. Sci.*, **33**, 2031–2048.
- , and —, 1978: Generalized Eliassen–Palm and Charney–Drazin theorems for waves on axisymmetric mean flows in compressible atmospheres. *J. Atmos. Sci.*, **35**, 175–185.
- , J. R. Holton, and C. B. Leovy, 1987: *Middle Atmosphere Dynamics*. Academic Press, 489 pp.
- Butchart, N., and E. E. Remsburg, 1986: The area of the stratospheric polar vortex as a diagnostic for tracer transport on an isentropic surface. *J. Atmos. Sci.*, **43**, 1319–1339.
- Charney, J. G., and P. G. Drazin, 1961: Propagation of planetary-scale disturbances from the lower into the upper atmosphere. *J. Geophys. Res.*, **66**, 83–109.
- Czaja, A., and J. Marshall, 2006: The partitioning of poleward heat transport between the atmosphere and ocean. *J. Atmos. Sci.*, **63**, 1498–1511.
- Edmon, H. J., B. J. Hoskins, and M. E. McIntyre, 1980: Eliassen–Palm cross sections for the troposphere. *J. Atmos. Sci.*, **37**, 2600–2616.
- Haynes, P. H., C. J. Marks, M. E. McIntyre, T. G. Shepherd, and K. P. Shine, 1991: On the “downward control” of extratropical diabatic circulations by eddy-induced mean zonal forces. *J. Atmos. Sci.*, **48**, 651–678.
- Held, I. M., and T. Schneider, 1999: The surface branch of the zonally averaged mass transport circulation in the troposphere. *J. Atmos. Sci.*, **56**, 1688–1697.
- Holton, J. R., 2004: *An Introduction to Dynamic Meteorology*. Academic Press, 535 pp.
- Iwasaki, T., 1989: A diagnostic formulation for wave-mean flow interactions and Lagrangian-mean circulation with a hybrid vertical coordinate of pressure and isentropes. *J. Meteor. Soc. Japan*, **67**, 293–312.
- , 1998: A set of zonal mean equations in a pressure–isentrope hybrid vertical coordinate. *J. Atmos. Sci.*, **55**, 3000–3002.
- Jukes, M., 2001: A generalization of the transformed Eulerian-mean meridional circulation. *Quart. J. Roy. Meteor. Soc.*, **127**, 147–160.
- , I. N. James, and M. Blackburn, 1994: The influence of Antarctica on the momentum budget of the southern extratropics. *Quart. J. Roy. Meteor. Soc.*, **120**, 1017–1044.
- Kanamitsu, M., W. Ebisuzaki, J. Woollen, S.-K. Yang, J. J. Hnilo, M. Fiorino, and G. L. Potter, 2002: NCEP–DOE AMIP-II Reanalysis (R-2). *Bull. Amer. Meteor. Soc.*, **83**, 1631–1643.
- Koh, T.-Y., and R. A. Plumb, 2004: Isentropic zonal average formalism and the near-surface circulation. *Quart. J. Roy. Meteor. Soc.*, **130**, 1631–1653.
- Kuo, A., R. A. Plumb, and J. Marshall, 2005: Transformed Eulerian-mean theory. Part II: Potential vorticity homogenization and the equilibrium of a wind- and buoyancy-driven zonal flow. *J. Phys. Oceanogr.*, **35**, 175–187.

- McIntosh, P. C., and T. J. McDougall, 1996: Isopycnal averaging and the residual mean circulation. *J. Phys. Oceanogr.*, **26**, 1655–1660.
- Nakamura, N., 1995: Modified Lagrangian-mean diagnostics of the stratospheric polar vortices. Part I. Formulation and analysis of GFDL SKYHI GCM. *J. Atmos. Sci.*, **52**, 2096–2108.
- , and D. Zhu, 2010: Finite-amplitude wave activity and diffusive flux of potential vorticity in eddy-mean flow interaction. *J. Atmos. Sci.*, **67**, 2701–2716.
- Pauluis, O., A. Czaja, and R. Korty, 2008: The global atmospheric circulation on moist isentropes. *Science*, **321**, 1075–1078.
- , —, and —, 2010: The global atmospheric circulation in moist isentropic coordinates. *J. Climate*, **23**, 3077–3093.
- , T. Shaw, and F. Laliberté, 2011: A statistical generalization of the transformed Eulerian-mean circulation for an arbitrary vertical coordinate system. *J. Atmos. Sci.*, **68**, 1766–1783.
- Peixoto, J. P., and A. H. Oort, 1992: *Physics of Climate*. AIP Press, 520 pp.
- Plumb, R. A., and J. D. Mahlman, 1987: The zonally averaged transport characteristics of the GFDL general circulation/transport model. *J. Atmos. Sci.*, **44**, 298–327.
- , and R. Ferrari, 2005: Transformed Eulerian-mean theory. Part I: Nonquasigeostrophic theory for eddies on a zonal-mean flow. *J. Phys. Oceanogr.*, **35**, 165–174.
- Schneider, T., 2005: Zonal momentum balance, potential vorticity dynamics, and mass fluxes on near-surface isentropes. *J. Atmos. Sci.*, **62**, 1884.
- Simmons, A. J., and D. M. Burridge, 1981: An energy and angular-momentum conserving vertical finite-difference scheme and hybrid vertical coordinates. *Mon. Wea. Rev.*, **109**, 758–766.
- Stachnik, J. P., and C. Schumacher, 2011: A comparison of the Hadley circulation in modern reanalyses. *J. Geophys. Res.*, **116**, D22102, doi:10.1029/2011JD016677.
- Tanaka, D., T. Iwasaki, S. Uno, M. Ujiie, and K. Miyazaki, 2004: Eliassen–Palm flux diagnosis based on isentropic representation. *J. Atmos. Sci.*, **61**, 2370–2383.
- Townsend, R. D., and D. R. Johnson, 1985: A diagnostic study of the isentropic zonally averaged mass circulation during the First GARP Global Experiment. *J. Atmos. Sci.*, **42**, 1565–1579.
- Tung, K. K., 1986: Nongeostrophic theory of zonally averaged circulation. Part I: Formulation. *J. Atmos. Sci.*, **43**, 2600–2618.